RSC Advances

PAPER

View Article Online
View Journal | View Issue

Cite this: *RSC Adv.*, 2022, **12**, 53

Preconcentration and determination of trace Hg(II) using ultrasound-assisted dispersive solid phase microextraction

Hilal Ahmad, *[ab] Bon Heun Koo[c] and Rais Ahmad Khan[d]

Received 26th October 2021
Accepted 13th December 2021

DOI: 10.1039/d1ra07898d

rsc.li/rsc-advances

Defect rich molybdenum disulfide (MoS_2) nanosheets were hydrothermally synthesized and their potential for ultrasound assisted dispersive solid phase microextraction of trace Hg(II) ions was assessed. Ultrasonic dispersion allows the MoS_2 nanosheets to chelate rapidly and evenly with Hg(II) ions and results in improving the precision and minimizing the extraction time. The multiple defect rich surface was characterized by X-ray diffraction and high-resolution transmission electron microscopy. The surface charge of intrinsically sulfur rich MoS_2 nanosheets and their elemental composition was characterized by zeta potential measurements, energy dispersive spectroscopy, and X-ray photoelectron spectroscopy. The cracks and holes on the basal planes of MoS_2 led to diffusion of the Hg(II) ions into the interior channels. Inner-sphere chelation along with outer-sphere electrostatic interaction were the proposed mechanism for the Hg(II) adsorption onto the MoS_2 surface. The experimental data showed good selectivity of MoS_2 nanosheets towards Hg(II) adsorption. The systematic and constant errors of the proposed method were ruled out by the analysis of the Standard Reference Material (>95% recovery with <5% RSD). The Student's *t*-test values for the analyzed Standard Reference Material were found to be less than the critical Student's *t* value at 95% confidence level. The limit of detection (3*S*) was found to be 0.01 ng mL^{-1}. The MoS_2 nanosheets were successfully employed for the analysis of Hg(II) in environmental water samples.

1. Introduction

Water pollution due to mercury contamination is an important environmental concern because of its potent detrimental impacts on biological systems, especially its potential lethal impacts on fish, birds and human health.[1–8] Thus, accurate analysis of Hg(II) in environmental and consumable water supplies remains a great challenge for public health and environmental protection.[9–12] Different methods and analytical techniques such as chemical treatment,[13] electrochemistry,[14] X-ray fluorescence,[15,16] inductively coupled plasma atomic/optical emission spectrometry[17,18] and inductively coupled plasma mass spectrometry[19,20] have been widely used for the analysis of Hg(II), however, direct determination of Hg(II) in real aqueous samples is challenging due to its very low concentrations with complex sample matrices.[21,22] The sample matrices compromise the instrumental detection, accuracy and the limit of quantification.[23,24] Nevertheless, this can be eliminated by sample pretreatment before analysis and thus, an extraction and preconcentration step is often pre-requisite to instrumental determination.[25–27] Considering the nanoadsorbents, solid phase microextraction and dispersive solid phase microextraction (DSPME) is one among the most promising approach for the separation and preconcentration of metal ions presented at trace or ultra-trace level in complex matrix solutions.[28–31] Traditional adsorbents such as ion exchange resin, zeolites, activated carbon and clays have been studied for the adsorption of mercury ions. However, these materials have inherent limitations for mercury extraction due to the poor selectivity, low adsorption capacity, use of high dose of adsorbent, and weak to poor binding affinity. Sulfur rich materials are the excellent adsorbents due to the strong Lewis soft acid–soft base interactions between the mercury and a sulfur site. A number of sulfur containing material have been recently reported to explore the substantial improvements in the adsorption of mercury ions.[32–34] For example, thiol functionalized metal organic frame works,[35,36] sulfur functionalized mesoporous carbon,[37] polymers functionalized with sulfur containing ligands,[38] metal chalcogenide aerogels[39] and layered metal sulfides.[40,41] Nonetheless, the major drawback is that these materials either involves the use of expensive raw materials (such as platinum salt, indium and zirconium) or suffers from sophisticated synthesis steps.

[a]*Division of Computational Physics, Institute for Computational Science, Ton Duc Thang University, Ho Chi Minh City, Vietnam. E-mail: hilalahmad@tdtu.edu.vn*
[b]*Faculty of Applied Sciences, Ton Duc Thang University, Ho Chi Minh City, Vietnam*
[c]*School of Materials Science and Engineering, Changwon National University, Changwon 51140, Gyeongnam, South Korea*
[d]*Department of Chemistry, College of Science, King Saud University, Riyadh-11451, Kingdom of Saudi Arabia*

Beside this, many of them shows relatively low adsorption capacity due to their low sulfur content or insufficient exposure of sulfur sites to metal ions. Consequently, considering the above challenges it is crucial to explore new adsorbents with advanced adsorption capacity, effective mercury binding sites and importantly, easy to synthesize.

Specifying the plenty of sulfur atoms in MoS_2 which could be a highly potential binding sites for mercury adsorption and assuming the 1 : 1 ratio of S/Hg, the theoretical adsorption capacity of MoS_2 nanosheets for mercury is estimated to be 2506 mg g^{-1}, which is highest among the best reported adsorbents till date.[27,33,34,36–38] In MoS_2, the Mo and S atom are covalently in-plane bonded forming a layered structure. The individual layers are weakly interacted with each other *via* van-der Waals forces in an out-of-plane manner, and can be easily dispersed upon ultrasonic treatment and therefore, make the internal sulfur sites accessible for Hg(II) binding.[42,43] Considering this, we synthesized a defect rich MoS_2 nanosheets and studied them for the first time to develop an ultra-sound assisted dispersive solid phase micro extraction (DSPME) method. The formation of defects on the basal planes of MoS_2 may induce the cracks and holes to diffuse the Hg(II) ions into the interior channels. The ultrasonic treatment of MoS_2 nanosheets not only allows a rapid, uniform and closer contact between the active sites of the sorbent and the mercury ions during the entrapping step but also favor the kinetics of mass-transfer and therefore enhance the efficacy and precision of the extraction method and reduces the extraction time. The extracted mercury ions after elution from the sorbent are determined by ICP-OES. In addition, this approach give rise to use lowest amount of sorbent in the range of micro to milligram. In consequences, the method was successfully applied to the accurate determination of mercury concentration in samples from laboratory to real life on a scale of μg L^{-1}.

2. Experimental

2.1 Reagents and solutions

Ammoniummolybdate and thiourea (99% purity) was purchased from Merck (China). Mercury solution (Hg(II); 1000 mg L^{-1} in 1% HNO_3) was obtained from Agilent (China). Other metal salts were purchased from Sigma-Aldrich (Germany) and used as received. Metal ion solutions were prepared through successive dilutions of the stock (1000 mg L^{-1}) with high purity water (18.2 MΩ cm) obtained from ultra-pure water system (Millipore). The Standard Reference Material (NIST 1641d) stored at −10 °C, was obtained from the national institute of standard and technology (Gaithersburg, USA) and was used after dilution.

2.2 Synthesis of MoS_2 nanosheets

A defect rich MoS_2 nanosheets was synthesized by a one-step hydrothermal method.[44] Briefly, a 2.0 g of ammoniummolybdate was dissolved with 2.5 g of thiourea in 150 mL of deionized water with vigorous magnetic stirring and transferred to a Teflon-lined autoclave (200 mL). The whole reaction mixture was kept in an air oven at 180 °C for 24 h. After cooling the hydrothermal assembly to the room temperature, the obtained grey–black color product was collected with the aid of centrifugation and washed repeatedly with ethanol and deionized water and dried at 60 °C in a vacuum oven for 6 h. The ICP-OES analyses was carried out to estimate the atomic ratio of Mo : S in the prepared material and was found to be 1 : 2.04.

2.3 Characterization of MoS_2 nanosheets

The X-ray powder diffraction (XRD) patterns of bulk and few layered MoS_2 were recorded on an X-ray diffractometer (XRD Smart Lab Guidance, Rigaku) equipped with Cu-Kα radiation (k = 1.5406 Å) in 2θ ranging from 10° and 60° at a scan rate of 5° min^{-1}. The surface morphology of MoS_2 nanosheets was characterized by high-resolution transmission electron microscopy (HRTEM, Techno, FEI). Samples were sputter-coated with palladium overlayer to avoid charging during the electron irradiation. Energy dispersive X-ray analysis (EDS) spectra for elemental analysis were obtained from an EDS analyzer (Bruker, Germany). The adsorption mechanism and valence state of the constituent elements were observed by X-ray photoelectron spectroscopy (XPS) (Thermo ESCALABA 250XI). Mercury ion concentrations were determined by inductively coupled plasma optical emission spectrometer (ICP-OES, PerkinElmer) at the axial mode of viewing plasma.

2.4 Optimized procedure for DSPME sample preparation

From a stock solution of MoS_2 suspension (5 mg in 100 mL of deionized water), a 1 mL aliquot of MoS_2 nanosheets was dropped to 25 mL of the polyethylene Falcon tube containing 10 mL of 50 μg L^{-1} of Hg(II) sample solution. The solution pH was adjusted to pH 6 by using 0.1 M of HNO_3 and 0.1 M NaOH. The whole reaction mixture was probe sonicated for 40 s. The act of sonication led to complete dispersion of MoS_2 nanosheets and considerably minimize the sample thickness, and eliminates the heap formation of nanosheets in the sample solution. Later, the sample solution was centrifuged at 4000 rpm for 60 s to collect the MoS_2 nanoadsorbent. Afterward, the MoS_2 nanoadsorbent with adsorbed Hg(II) was agitated ultrasonically with

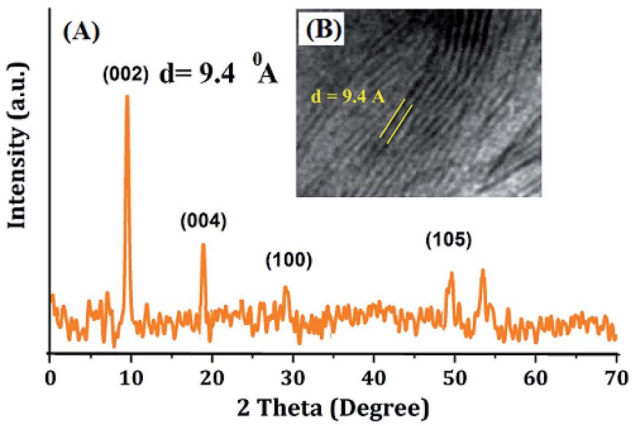

Fig. 1 (A) XRD pattern and (B) cross sectional HRTEM image of MoS_2.

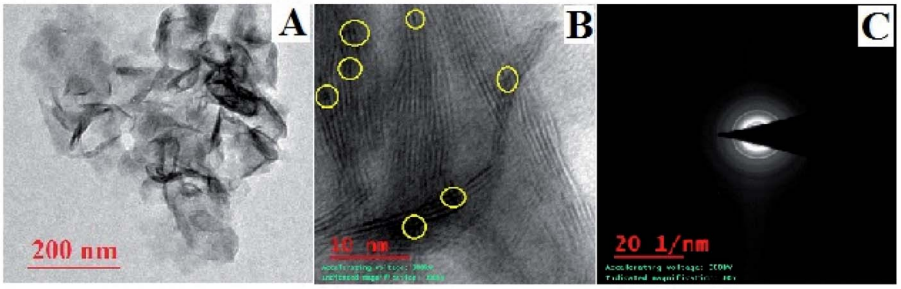

Fig. 2 HRTEM images of (A) MoS_2 nanosheets; (B) basal plane of MoS_2 showing fine structures; (C) corresponding SAED diffraction patterns of MoS_2.

5 mL of 1.0 M nitric acid for 60 s to elute the sorbed Hg(II). The whole reaction vial was centrifuged to separate both the phases. The eluent with Hg(II) was gathered and evaluated by ICP-OES to identify the Hg(II) concentration.

3. Results and discussion

3.1 Characterization

The prepared defect rich MoS_2 nanosheets were systematically investigated for the structural features and composition studies. The XRD pattern of the synthesized MoS_2 was evaluated and presented in Fig. 1. The appearance of two diffraction peaks at low-angle region (9.8° and 19.4°, Fig. 1), centered at (*hkl*) (002) and (004), indicates the formation of lamellar structures with enlarge interlayer spacing, corresponds to *d*-spacing values of 9.4 Å. Fig. 2A and B shows the HRTEM image of MoS_2 nanosheets, illustrates the fine sheets with defect rich surface (encircle with yellow color) along the basal planes, evident by the presence of abundant dislocations and distortions. The defect-rich features was further confirmed by the corresponding selected area electron diffraction (SAED) pattern (Fig. 2C). The corresponding cross-sectional HRTEM image (inset of Fig. 1) shows the interlayer spacing with a value of 9.4 Å, which is far beyond the interlayer spacing values of bulk MoS_2 (6.24 Å). Such an important interlayer elaboration between the two neighboring S–Mo–S sheets could fully expose the interior space of MoS_2. The interior surface possess large number of active sulfur sites are now available for Hg(II) binding, which were before inaccessible as in case of bulk MoS_2. Moreover, the surface defects presented on the basal planes promotes the diffusion of Hg(II) ions to the interior channels of MoS_2 nanosheets. Fig. 3 shows the elemental mapping of MoS_2 after Hg(II) adsorption, observed from the FESEM image, illustrates the presence of Hg(II) along with Mo and S contents, supports the potential adsorption of Hg(II) onto the MoS_2 nanosheets. To understand the adsorption mechanism and the oxidation state of the constituent elements, the wide scan XPS spectra with deconvolution of the core-level peaks were carried out using monochromatic Al K alpha light at 1486.6 eV and an emission angle of 45 with spot size of 500 μm. The XPS analysis data for MoS_2 obtained after Hg(II) adsorption were given in Table 1. Fig. 4A shows the comparative XPS survey spectrum of MoS_2 before and after Hg(II) adsorption, indicates the peaks for Mo, S and Hg at characteristics binding energies. In Fig. 4B, the deconvoluted peaks at the binding energy of 230.8 and 233.9 eV are assigned to the Mo $3d_{5/2}$ and Mo $3d_{3/2}$ element, respectively. The deconvoluted peaks of S 2p element of MoS_2 before and after Hg(II) adsorption were shown in Fig. 4C. The characteristic peaks of S observed at binding energy values of 161.5 and 162.6 eV, were assigned to S $2p_{3/2}$ and S $2p_{1/2}$. After Hg(II) adsorption these S peaks shows a shift to higher binding energies *c.a* at 161.7 and 163.0 eV, indicates their binding with Hg(II) ions (Fig. 4C). Such a blue shift in binding energies of the

Table 1 XPS data of MoS_2 nanosheets

Element	Peak position (eV)	FWHM	Area(P) cps	Atomic%
Mo 3d	230.8	0.87	144 917.0	22.04
S 2s	228.0	1.63	18 545.2	23.86
S 2p	161.8	1.05	58 622.5	54.10

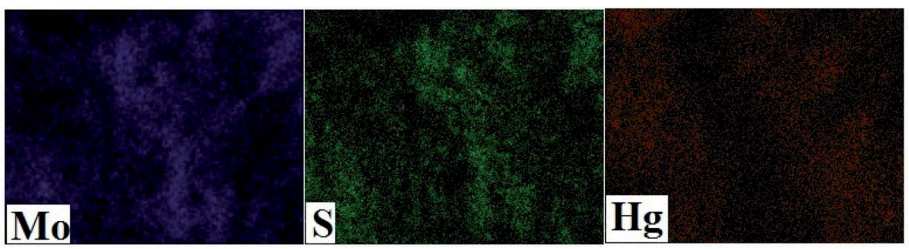

Fig. 3 Elemental mapping of MoS_2 after Hg(II) adsorption.

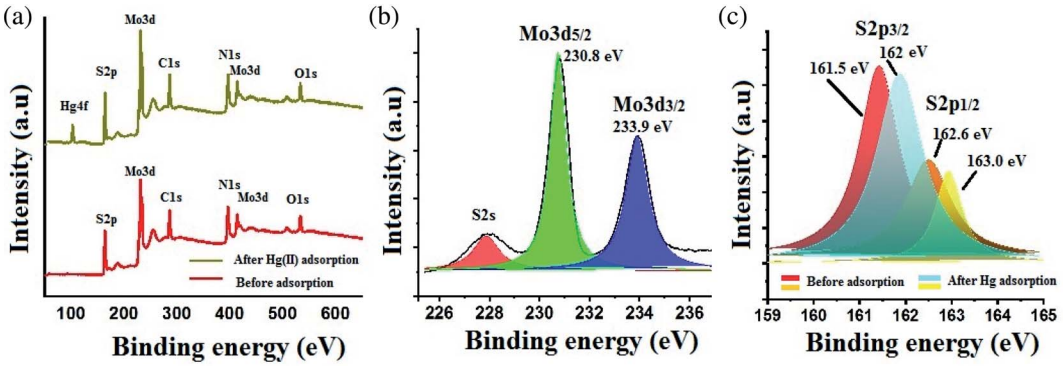

Fig. 4 (a) XPS survey spectra of MoS_2 before and after Hg(II) adsorption; (b) deconvoluted Mo 3d peaks of MoS_2; (c) deconvoluted S 2p peaks before and after Hg(II) adsorption illustrates a shift in binding energies.

S peaks after Hg(II) adsorption was mainly due to the interaction of MoS_2 with Hg(II) ions and thereby resulting in the disparity of the XPS spectra before Hg(II) adsorption.

3.2 Optimization of experimental conditions

A univariate approach was employed to optimize the important experimental parameters to develop a dispersive solid phase microextraction method using MoS_2 nanosheets.

3.2.1 Effect of the solution pH. The sample pH is an important parameter for the adsorption of metal ions, considering that it influences both the distribution of surface charge of adsorbent and the metal ion species. The impact of solution pH on the adsorption of Hg(II) onto MoS_2 nanosorbent was studied at the pH range of 1–7 with initial Hg(II) concentration of 10 000 μg L^{-1}. For comparison purpose the sorption of Hg(II) at low level concentration (100 μg L^{-1}) was also studied. The observed data are shown in Fig. 5. The Hg(II) sorption beyond pH 7 was avoided due to the precipitation of Hg(II) in basic medium. Also the adsorption/influence of typical alkali and alkaline earth metal which were potentially co-exist with the Hg(II) has been also studied. From Fig. 5, it could be seen that, at higher Hg(II) concentration the adsorption of Hg(II) onto MoS_2 varies at different sample pH. Moreover, at low Hg(II) concentration, no significant effect of sample pH on Hg(II) adsorption was observed (Fig. 5). The adsorption efficiency of Hg(II) increases with the increase of sample pH and reached to maxima at pH 6–7. The surface charge of MoS_2 played an important role in the physico-chemical adsorption.[45,46] From the zeta potential studies of MoS_2, the isotropic electric point (pH_z) of MoS_2 was observed below to pH 1.0 (Fig. 5), indicates that the surface was negatively charged at pH above 1.0 and the sulfur sites are available for chelation with metal ions.[47] However, at lower pH values, the concentration of hydrogen ions (counter ion) is high enough to compete with Hg(II), due to such competition with counter ions, a decrease in adsorption of Hg(II) was observed. However, above pH 4, the sulfur ions becomes deprotonated and the Hg(II) adsorption significantly increases and reaches to maximum at pH 6–7. According to Lewis hard and soft acid base concept, the Hg–S chelate formation could be a primary adsorption pathway due to the most favorable soft–soft Hg–S interaction.[48–51] Moreover, Hg(II) ions could binds with two sulfur ions to form a chelate at low Hg(II) concentration and with one sulfur ion at higher Hg(II) concentration to form inner-sphere complex, in addition to the outer layer electrostatic interaction between the Hg(II) and negatively charge MoS_2 surface.[51,52] Thus, MoS_2 nanosheets shows a multi-layer adsorption phenomenon, although the physical adsorption might be of minor contribution compared to chemisorption. In conclusion, pH 6 was optimized for Hg(II) extraction in further DSPME experiments. Moreover, no considerable hindrance in the DSPME/adsorption of Hg(II) (100 ppb) was observed in presence of Na^+, K^+, Ca^{2+}, Mg^{2+}, Cl^-, CO_3^{2-}, NO_3^{2-}, SO_4^{2-} and PO_4^{2-} ions at varying concentrations (0.25 and 0.5 M) (Fig. 6). This indicates the specific adsorption of Hg(II) onto MoS_2 surface over these co-ions. This selective uptake might be due to the strong soft–soft interactions between Hg(II) and sulfur ions of the adsorbent.

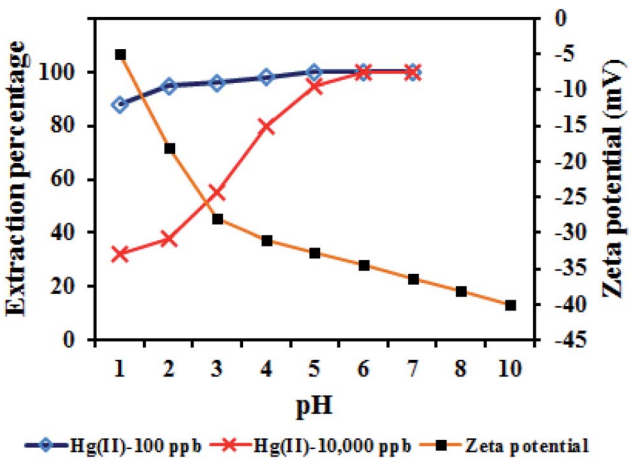

Fig. 5 Effect of sample pH on Hg(II) adsorption at higher (10 000 ppb) and lower (100 ppb) concentrations.

3.2.2 Effect of the sonication time. To optimized the sonication step for complete adsorption of Hg(II) ions, a series of experiments was conducted with 1.0 mg of MoS_2, ultrasonicated with 10 mL of Hg(II) solution (1 mg L^{-1}) at pH 6 at

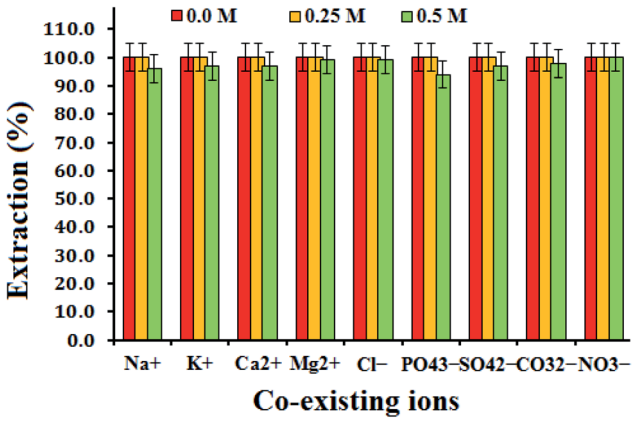

Fig. 6 Effect of co-existing ions at varying concentrations on the adsorption of Hg(II) by MoS_2 adsorbent (Hg(II) 100 μg L^{-1}; adsorbent dosage 1.0 mg; sample vol. 10 mL).

varying time intervals of 10 to 100 seconds (probe sonication; power 40 W in continuous mode). The adsorbed Hg(II) ions was eluted with 5 mL of 1.0 M HNO_3 and the two phases was separated by centrifugation at 4000 rpm for 60 s. The Hg(II) concentration was measured by ICP-OES. The ultrasonication compared to stirring and shaking increases the area to volume ratio of nanoadsorbent by exfoliating the MoS_2 nanosheets, and therefore enhanced the metal ion adsorption by exposing the hidden active sites. The results are presented in Fig. 7A, shows the gradual increase of Hg(II) adsorption percentage in first 30 s and the complete extraction (100%) was observed from 40 s and upwards up to a sonication time of 100 s. Hence, a 40 s of sonication step was optimized for all further studies.

3.2.3 Effect of the adsorbent dose. In DSPME, the optimum amount of solid to be taken is of great importance in order to disperse them completely in a given sample volume and to ensure the complete retention of analyte ions. Considering this, the solid-to-liquid (S/L) ratio has been optimized by carried out multiple sets of experiments. To this job, varying amount of solid MoS_2 (100–1200 μg) were disperse in 10 mL of the model Hg(II) solutions (50 mg L^{-1}) in 25 mL of polyethylene falcon tubes. The whole reaction setups were sonicated for 40 s and the sorbed Hg(II) ions were eluted using 5 mL of 1.0 M nitric acid and subsequently determine by ICP-OES. The results are presented in Fig. 7B. The optimum S/L ratio of MoS_2, where the complete adsorption of Hg(II) achieved, was found at 60 μg mL^{-1}, and the same was used for further experiments.

3.2.4 Effect of trace Hg(II) concentration. Several real samples possess trace levels of Hg(II) concentrations and challenge their direct instrumental determination. Thus, requires a sample preparation/preconcentration step before analysis. To analyse the effect of lower Hg(II) concentration, a bench of samples containing varying Hg(II) concentration (0.01–2.0 μg L^{-1}) were set to pH of 6 using 0.1 M of HNO_3 and 0.1 M NaOH. The sample solution was mixed with 0.5 mg of MoS_2 adsorbent and were ultrasonicated for 40 s. To separate both the phases (adsorbent and solution) the whole sample was centrifuged at 4000 rpm for 60 s. The obtained MoS_2 sheets were added with 5 mL of 1 M HNO_3 to elute the adsorbed Hg(II) followed by sonication and centrifugation and ultimately analyzed by ICP-OES to determine the Hg(II). The experiment was repeated thrice ($n = 3$) and the results are shown in Fig. 7C. The obtained data suggest that the Hg(II) at the concentration above 0.2 μg L^{-1} was successfully recovered (recovery > 99%), however, for the samples contained 0.15, 0.1 and 0.01 μg L^{-1} of Hg(II), the mean recovery percentage was decreased to 82, 75 and 68%, respectively, indicates incomplete adsorption of Hg(II) ions due to very low amount of analyte ions. In conclusion, the proposed DSPME method could preconcentrate and quantitavely determined the trace Hg(II) ions down to 0.2 μg L^{-1}.

3.3 Desorption and reusability studies

Considering the reusability of the adsorbent, various stripping agent such as hydrochloric and nitric acids at different molar concentrations (0.5–1.5 M) and volumes (1–5 mL) were studied to elute the adsorbed Hg(II) ions. The Hg(II) loaded adsorbent (10 mg of MoS_2) was mixed with studied eluent and sonicated for 40 s following the centrifugation to gather the eluent and subsequently analysed by ICP-OES. The results are presented in Fig. 8. Among the studied eluent it was found that the 5 mL of 1 M hydrochloric acid eluted 88% of adsorbed ions while nitric acid with same volume and concentration adequately eluted 100% of Hg(II) ions. The whole procedure of quantitative desorption of mercury ions was repeated for 3 times and

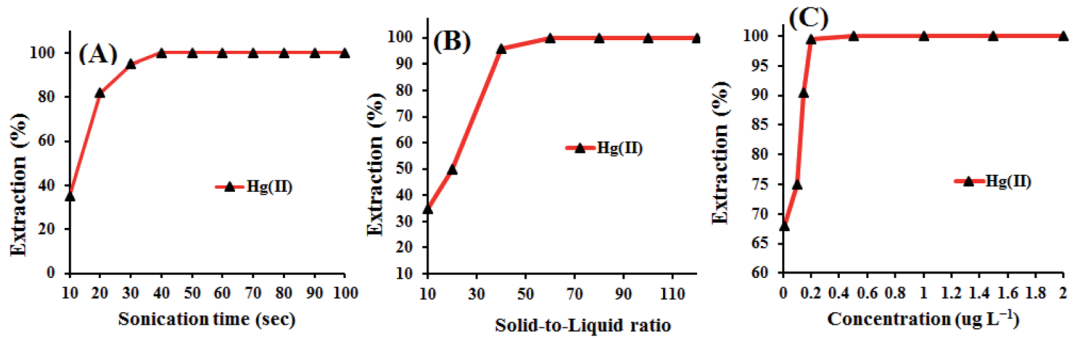

Fig. 7 (A) Effect of sonication time on the adsorption Hg(II) (adsorbent dose 1.0 mg; Hg(II) conc. 1 mg L^{-1}); (B) effect of adsorbent dose; and (C) effect of trace Hg(II) concentration (0.01–2.0 μg L^{-1}).

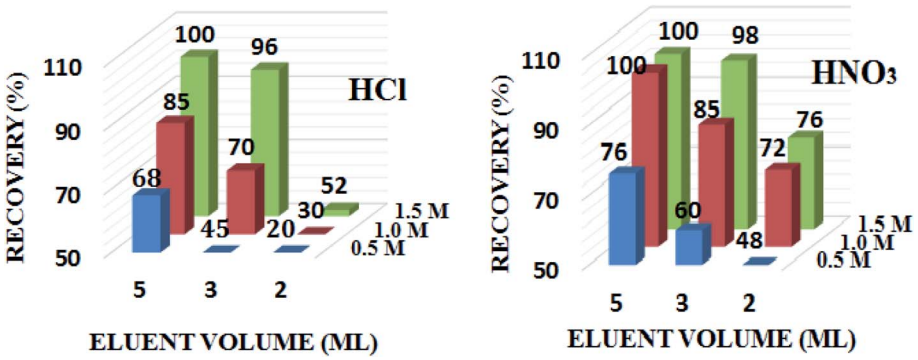

Fig. 8 Effect of eluent concentration and volume.

Table 2 DMSPE method validation by analyzing standard reference material for Hg(II) ion determination

Samples	Certified value (μg L^{-1})	Value found after DMSPE method[a] (μg L^{-1}) ± standard deviation	Value of *t*-test[b]
NIST SRM 1641d	Hg(II): 1.56 ± 0.02	1.55 ± 0.03	2.14

[a] Mean value for $N = 3$. [b] At 95% confidence limit; $t_{critical} = 4.303$.

achieved the recovery > 99.9%, for all sets. Therefore, 5 mL of 1 M nitric acids were used as eluent in all experiments.

The reusability of the same set of adsorbent was examined to check the method stability. A suitable amount of MoS_2 adsorbent (0.5 mg) was mixed with 10 mL of Hg(II) solution (10 μg L^{-1}). After sonication step, the uptake Hg(II) got eluted using 3 mL of 1 M nitric acids and consequently determined by ICP-OES. The sorption/desorption experiments was repeated several times with the same set of adsorbent. The obtained results suggest that the MoS_2 nanosheets can be reused up to 40 cycles without substantial loss in the adsorption performance. The recovery of Hg(II) ions up to 40 cycles is above 98%, afterward considerable loss in the adsorption of Hg(II) (recovery < 94%) was observed. This might due to the aggregation and/or structural decomposition of the MoS_2 nanosheets.

3.4 Analytical figures of merit

Standard Reference Materials (NIST SRM 1641d) was analysed to evaluate the accuracy of the proposed methodology (Table 2). The Student's *t*-test value computed for Hg(II) was found less than the critical Student's *t*-test value of 4.303 for $N = 3$ at 95% confidence limit. The results presented in Table 2 shows the closeness of the agreement between the measured and a true value without any systematic errors, since the mean Hg(II) concentration value obtained with DMSPE method were statistically insignificant with the reported/certified value. Moreover, the calibration plot obtained by the method of least square, after preconcentrating the standards in the concentration range of 0.3–1000 μg L^{-1}, was found linear with the determination coefficient (R^2) of 0.9998 for the regression equation $y = 1184.08x - 489.62$, at the wavelength of 253.652 nm. To evaluate the intra-day precision of the method, ten replicate samples of 1.0 μg L^{-1} of Hg(II) was analyzed following the DSPME procedure. The relative standard deviation for replicate measurements was found to be 3.2%, indicates the acceptable closeness of repeated measurements. Similarly, the inter-day precision for the analysis of ten replicate samples of 1.0 μg L^{-1} of Hg(II) for ten consecutive days was found to be 3.8%. Considering the IUPAC guidelines,[53] the limit of detection (LOD) (3*S*) of the proposed DSPME method was found to be 0.01 ng mL^{-1} for Hg(II) ions, indicates their potential application in real sample analysis. The LOD was calculated as the concentration of Hg(II)

Table 3 A comparative overview of analytical performance data with literatures

Materials used	Method	LODs (ng mL^{-1})	Technique	References
MoS_2 nanosheets	Dispersive solid phase extraction	0.01	ICP-OES	This work
Functionalized graphene oxide	Magnetic solid-phase extraction	0.05	ICP-OES	54
Fe_3O_4@graphene oxide	Magnetic dispersive solid phase extraction	0.25	GFAAS	55
PANI-MoS_2	Solid phase extraction	0.06	ICP-OES	56
Functionalized cellulose nanofibers	Solid phase extraction	0.09	ICP-OES	57
Functionalized magnetic nanoparticles	Magnetic solid-phase extraction	0.22	HR CS ETAAS	58

Table 4 Determination of Hg(II) ions concentration in real samples using ICP-OES after DMSPE

Samples	Amount added (μg)	Amount found (μg L^{-1}) ± standard deviation[a]	Recovery percent (RSD)[c]	Value of *t*-test[d]
Tap water	0	ND[b]	—	—
	5	5.00 ± 0.26	100 (0.05)	0.16
	10	9.98 ± 0.42	99.8 (0.08)	1.53
Industrial effluent	0	6.28 ± 0.08	—	1.55
	5	11.27 ± 0.76	99.8 (0.15)	1.23
	10	16.30 ± 0.83	100.2 (2.06)	1.45
River water	0	5.13 ± 0.50	—	1.50
	5	10.13 ± 0.92	100 (0.10)	1.16
	10	15.12 ± 1.53	99.9 (1.18)	2.36

[a] $N = 3$. [b] Not detected. [c] Relative standard deviation. [d] At 95% confidence level, $t_{critical} = 4.303$.

gives a signal intensity equivalent to 3 times the standard deviation of mean blank signal (0.0033 ± 10) of 20 replicate blank measurements (*i.e.* 3*S*). The robustness of the method was evaluated by altering the sample pH from 6 to 6 ± 0.5 and the sonication time of 40 s to 40 ± 5 s. No considerable adjustment in the adsorption and recovery of Hg(II) was observed. Furthermore, the suggested approach had no significant drawbacks, and the analytical figures of merit associated with previous reported methods either used nanomaterials or other adsorbents in conjunction with ICP-OES or other sophisticated detection techniques are compared and summarized in Table 3. The present method has comparable or even better detection limit than previous reported methods combined with GFAAS, ICP-OES, and ETAAS detection techniques.[54–58]

3.5 Real sample analysis

Tap water, industrial effluent and river water samples was successfully enriched under optimized experimental conditions and the concentration of Hg(II) ions was determined by ICP-OES. The Hg(II) contamination in industrial effluent and river water samples was found to be 6.28 and 5.13 μg L^{-1}, respectively. The results are illustrated in Table 4. The integrity of the approach was checked out by spiking the samples with recognized amounts of Hg(II) at two different degrees (5 and 10 μg). Recoveries of the spiked Hg(II) ions were ascertained by measuring the recovered amount from the real samples with a 95% confidence level. The mean percentage recoveries of the added Hg(II) were 99.8–100.2% with an RSD ranging 0.05–2.06% for the spiked amount of Hg(II).

4. Conclusion

Two dimensional MoS_2 nanosheets with widened interlayer spacing could be easily synthesized by hydrothermal method without using any intercalating agents. The material shows excellent selectivity towards Hg(II) with fast adsorption performance. Due to inherent sulfur rich characteristic and large interlayer spacing, the MoS_2 nanosheets advantageously utilized in the DSPME of trace Hg(II) from aqueous samples. The main possible mechanism for the Hg(II) adsorption could be the strong Hg(II)–S complexation along with the electrostatic interaction. The MoS_2 nanosheets was efficient enough for quantitative analyses of the trace Hg(II) on a scale of ng mL^{-1} without the interference of common co-existing ions. The applicability of the proposed DMSPE method in the extraction and determination of Hg(II) has been verified by analyzing the real water and industrial wastewater samples.

Conflicts of interest

There are no conflicts to declare.

Acknowledgements

The work was supported by the researchers project number (RSP-2021/400), King Saud University, Riyadh, Saudi Arabia.

References

1 G. R. Golding, C. A. Kelly, R. Sparling, P. C. Loewen and T. Barkay, Evaluation of Mercury Toxicity as a Predictor of Mercury Bioavailability, *Environ. Sci. Technol.*, 2007, **41**(16), 5685–5692.
2 A. Asaduzzaman, D. Riccardi, A. T. Afaneh, S. J. Cooper, J. C. Smith, F. Wang, J. M. Parks and G. Schreckenbach, Environmental Mercury Chemistry – In Silico, *Acc. Chem. Res.*, 2019, **52**(2), 379–388.
3 E. Gertz, Study reveals new mercury risks for fish and birds, *Environ. Sci. Technol.*, 2009, **43**(24), 9048–9049.
4 A. K. James, S. Nehzati, N. V. Dolgova, D. Sokaras, T. Kroll, K. Eto, J. L. O'Donoghue, G. E. Watson, G. J. Myers, P. H. Krone, I. J. Pickering and G. N. George, Rethinking the Minamata Tragedy: What Mercury Species Was Really Responsible?, *Environ. Sci. Technol.*, 2020, **54**(5), 2726–2733.
5 R. Sulaiman, M. Wang and X. Ren, Exposure to Aluminum, Cadmium, and Mercury and Autism Spectrum Disorder in Children: A Systematic Review and Meta-Analysis, *Chem. Res. Toxicol.*, 2020, **33**(11), 2699–2718.
6 M. Wang, J.-S. Lee and Y. Li, Global Proteome Profiling of a Marine Copepod and the Mitigating Effect of Ocean

Acidification on Mercury Toxicity after Multigenerational Exposure, *Environ. Sci. Technol.*, 2017, **51**(10), 5820–5831.

7 J. Zhou, D. Obrist, A. Dastoor, M. Jiskra and A. Ryjkov, Vegetation uptake of mercury and impacts on global cycling, *Nat. Rev. Earth Environ.*, 2021, **2**(4), 269–284.

8 D. Hou, D. O'Connor, A. D. Igalavithana, D. S. Alessi, J. Luo, D. C. W. Tsang, D. L. Sparks, Y. Yamauchi, J. Rinklebe and Y. S. Ok, Metal contamination and bioremediation of agricultural soils for food safety and sustainability, *Nat. Rev. Earth Environ.*, 2020, **1**(7), 366–381.

9 I. L. Gunsolus and C. L. Haynes, Analytical Aspects of Nanotoxicology, *Anal. Chem.*, 2016, **88**(1), 451–479.

10 S. D. Richardson and T. A. Ternes, Water Analysis: Emerging Contaminants and Current Issues, *Anal. Chem.*, 2014, **86**(6), 2813–2848.

11 J. Johnson, Where goes the missing mercury?, *Chem. Eng. News Arch.*, 2004, **82**(11), 31–32.

12 J. Wu, M. Cao, D. Tong, Z. Finkelstein and E. M. V. Hoek, A critical review of point-of-use drinking water treatment in the United States, *npj Clean Water*, 2021, **4**(1), 40.

13 C. Y. Teh, P. M. Budiman, K. P. Y. Shak and T. Y. Wu, Recent Advancement of Coagulation–Flocculation and Its Application in Wastewater Treatment, *Ind. Eng. Chem. Res.*, 2016, **55**(16), 4363–4389.

14 Z. Hu, U. Kurien, K. Murwira, A. Ghoshdastidar, O. Nepotchatykh and P. A. Ariya, Development of a Green Technology for Mercury Recycling from Spent Compact Fluorescent Lamps Using Iron Oxides Nanoparticles and Electrochemistry, *ACS Sustainable Chem. Eng.*, 2016, **4**(4), 2150–2157.

15 Y. Wang, L. Zhang, X. Han, L. Zhang, X. Wang and L. Chen, Fluorescent probe for mercury ion imaging analysis: Strategies and applications, *Chem. Eng. J.*, 2021, **406**, 127166.

16 X. Wang, Z. Jiang, C. Yang, S. Zhen, C. Huang and Y. Li, Facile synthesis of binary two-dimensional lanthanide metal–organic framework nanosheets for ratiometric fluorescence detection of mercury ions, *J. Hazard. Mater.*, 2022, **423**, 126978.

17 M. Hossain, D. Karmakar, S. N. Begum, S. Y. Ali and P. K. Patra, Recent trends in the analysis of trace elements in the field of environmental research: A review, *Microchem. J.*, 2021, **165**, 106086.

18 L. Qian, Z. Lei, X. Peng, G. Yang and Z. Wang, Highly sensitive determination of cadmium and lead in whole blood by electrothermal vaporization-atmospheric pressure glow discharge atomic emission spectrometry, *Anal. Chim. Acta*, 2021, **1162**, 338495.

19 E. Bozorgzadeh, A. Pasdaran and H. Ebrahimi-Najafabadi, Determination of toxic heavy metals in fish samples using dispersive micro solid phase extraction combined with inductively coupled plasma optical emission spectroscopy, *Food Chem.*, 2021, **346**, 128916.

20 S. Kulomäki, E. Lahtinen, S. Perämäki and A. Väisänen, Determination of mercury at picogram level in natural waters with inductively coupled plasma mass spectrometry by using 3D printed metal scavengers, *Anal. Chim. Acta*, 2019, **1092**, 24–31.

21 J. L. M. Viana, A. A. Menegário and A. H. Fostier, Preparation of environmental samples for chemical speciation of metal/metalloids: A review of extraction techniques, *Talanta*, 2021, **226**, 122119.

22 Y. Song, Q. Ma, H. Cheng, J. Liu and Y. Wang, Simultaneous enrichment of inorganic and organic species of lead and mercury in pg L^{-1} levels by solid phase extraction online combined with high performance liquid chromatography and inductively coupled plasma mass spectrometry, *Anal. Chim. Acta*, 2021, **1157**, 338388.

23 J. G. Dunn, D. Philips and W. van Bronswijk, An Exercise To Illustrate the Importance of Sample Preparation in Chemical Analysis, *J. Chem. Educ.*, 1997, **74**(10), 1188.

24 G. L. Donati, M. C. Santos, A. P. Fernandes and J. A. Nóbrega, Sampling and Sample Homogeneity as Introductory Topics in Analytical Chemistry Undergraduate Courses, *Spectrosc. Lett.*, 2008, **41**(5), 251–257.

25 J.-j. Fei, X.-h. Wu, Y.-l. Sun, L.-y. Zhao, H. Min, X.-b. Cui, Y.-j. Chen, S. Liu, H.-z. Lian and C. Li, Preparation of a novel amino functionalized ion-imprinted hybrid monolithic column for the selective extraction of trace copper followed by ICP-MS detection, *Anal. Chim. Acta*, 2021, **1162**, 338477.

26 J. Yang, Y. Zhang, J. Guo, Y. Fang, Z. Pang and J. He, Nearly Monodisperse Copper Selenide Nanoparticles for Recognition, Enrichment, and Sensing of Mercury Ions, *ACS Appl. Mater. Interfaces*, 2020, **12**(35), 39118–39126.

27 Y. Wang, Q. Dang, C. Liu, D. Yu, X. Pu, Q. Wang, H. Gao, B. Zhang and D. Cha, Selective Adsorption toward Hg(II) and Inhibitory Effect on Bacterial Growth Occurring on Thiosemicarbazide-Functionalized Chitosan Microsphere Surface, *ACS Appl. Mater. Interfaces*, 2018, **10**(46), 40302–40316.

28 N. Reyes-Garcés, E. Gionfriddo, G. A. Gómez-Ríos, M. N. Alam, E. Boyacı, B. Bojko, V. Singh, J. Grandy and J. Pawliszyn, Advances in Solid Phase Microextraction and Perspective on Future Directions, *Anal. Chem.*, 2018, **90**(1), 302–360.

29 L. Jiang, Y. Li, X.-a. Yang, C.-z. Jin and W.-b. Zhang, Ultrasound-assisted dispersive solid phase extraction for promoting enrichment of ng L^{-1} level Hg^{2+} on ionic liquid coated magnetic materials, *Anal. Chim. Acta*, 2021, **1181**, 338906.

30 N. Baghban, E. Yilmaz and M. Soylak, A magnetic MoS_2-Fe_3O_4 nanocomposite as an effective adsorbent for dispersive solid-phase microextraction of lead(II) and copper(II) prior to their determination by FAAS, *Microchim. Acta*, 2017, **184**(10), 3969–3976.

31 N. Baghban, E. Yilmaz and M. Soylak, Nanodiamond/MoS_2 nanorod composite as a novel sorbent for fast and effective vortex-assisted micro solid phase extraction of lead(II) and copper(II) for their flame atomic absorption spectrometric detection, *J. Mol. Liq.*, 2017, **234**, 260–267.

32 B. Manna and C. R. Raj, Nanostructured Sulfur-Doped Porous Reduced Graphene Oxide for the Ultrasensitive Electrochemical Detection and Efficient Removal of Hg(II), *ACS Sustainable Chem. Eng.*, 2018, **6**(5), 6175–6182.

33 F. He, W. Wang, J.-W. Moon, J. Howe, E. M. Pierce and L. Liang, Rapid Removal of Hg(II) from Aqueous Solutions Using Thiol-Functionalized Zn-Doped Biomagnetite Particles, *ACS Appl. Mater. Interfaces*, 2012, **4**(8), 4373–4379.

34 M. R. Khan and S. B. Khoo, Epoxy-Graphite Tube Bulk-Modified with 2-Mercaptobenzothiazole as a Robust Electrode for the Preconcentration and Stripping Analysis of Hg(II), *Anal. Chem.*, 1996, **68**(18), 3290–3294.

35 B. Li, Y. Zhang, D. Ma, Z. Shi and S. Ma, Mercury nano-trap for effective and efficient removal of mercury(II) from aqueous solution, *Nat. Commun.*, 2014, **5**(1), 5537.

36 C. W. Abney, J. C. Gilhula, K. Lu and W. Lin, Metal–Organic Framework Templated Inorganic Sorbents for Rapid and Efficient Extraction of Heavy Metals, *Adv. Mater.*, 2014, **26**(47), 7993–7997.

37 M. M. Rao, D. H. K. K. Reddy, P. Venkateswarlu and K. Seshaiah, Removal of mercury from aqueous solutions using activated carbon prepared from agricultural by-product/waste, *J. Environ. Manage.*, 2009, **90**(1), 634–643.

38 B. Aguila, Q. Sun, J. A. Perman, L. D. Earl, C. W. Abney, R. Elzein, R. Schlaf and S. Ma, Efficient Mercury Capture Using Functionalized Porous Organic Polymer, *Adv. Mater.*, 2017, **29**(31), 1700665.

39 J. Guo, H. Tian, J. Yang and J. He, Self-assembly of mercury-ion recognizing CuS nanocrystals into 3D sponge-like aerogel towards superior mercury capturer with outstanding selectivity and efficiency, *Chem. Eng. J.*, 2021, **426**, 130868.

40 X. Xie, Z. Zhang, Z. Chen, J. Wu, Z. Li, S. Zhong, H. Liu, Z. Xu and L. Zhilou, *In situ* preparation of zinc sulfide adsorbent using local materials for elemental mercury immobilization and recovery from zinc smelting flue gas, *Chem. Eng. J.*, 2021, 132115.

41 W. Fu, H. Chen, S. Yang, W. Huang and Z. Huang, Poly(diallyldimethylammonium-MoS_4) based amorphous molybdenum sulphide composite for selectively mercury uptake from wastewater across a large pH region, *Chemosphere*, 2019, **232**, 9–17.

42 J.-Y. Kim, J. D. Kim, J.-H. Kim, S.-K. Kim and J.-M. Lee, Effects of ultrasonic dispersion on nanoparticle based polyurethane foam reinforcement, *Polym. Test.*, 2021, **99**, 107210.

43 A. Azari, M. Yeganeh, M. Gholami and M. Salari, The superior adsorption capacity of 2,4-Dinitrophenol under ultrasound-assisted magnetic adsorption system: Modeling and process optimization by central composite design, *J. Hazard. Mater.*, 2021, **418**, 126348.

44 E. Yilmaz and G. Sarp, Graphene-like MoS_2-modified magnetic C-dot nanoflowers: an efficient magnetic solid-phase extraction adsorbent for monitoring of trace amounts of ibuprofen, *Anal. Methods*, 2020, **12**(12), 1570–1578.

45 S. S. Chou, M. De, J. Kim, S. Byun, C. Dykstra, J. Yu, J. Huang and V. P. Dravid, Ligand Conjugation of Chemically Exfoliated MoS_2, *J. Am. Chem. Soc.*, 2013, **135**(12), 4584–4587.

46 X. Chen, N. C. Berner, C. Backes, G. S. Duesberg and A. R. McDonald, Functionalization of Two-Dimensional MoS_2: On the Reaction Between MoS_2 and Organic Thiols, *Angew. Chem., Int. Ed.*, 2016, **55**(19), 5803–5808.

47 Z. Wang and B. Mi, Environmental Applications of 2D Molybdenum Disulfide (MoS_2) Nanosheets, *Environ. Sci. Technol.*, 2017, **51**(15), 8229–8244.

48 R. G. Pearson, Hard and soft acids and bases, HSAB, part II: Underlying theories, *J. Chem. Educ.*, 1968, **45**(10), 643.

49 R. G. Pearson, Hard and soft acids and bases, HSAB, part 1: Fundamental principles, *J. Chem. Educ.*, 1968, **45**(9), 581.

50 P. K. Chattaraj, H. Lee and R. G. Parr, HSAB principle, *J. Am. Chem. Soc.*, 1991, **113**(5), 1855–1856.

51 K. Ai, C. Ruan, M. Shen and L. Lu, MoS_2 Nanosheets with Widened Interlayer Spacing for High-Efficiency Removal of Mercury in Aquatic Systems, *Adv. Funct. Mater.*, 2016, **26**(30), 5542–5549.

52 S. J. L. Billinge, E. J. McKimmy, M. Shatnawi, H. Kim, V. Petkov, D. Wermeille and T. J. Pinnavaia, Mercury Binding Sites in Thiol-Functionalized Mesostructured Silica, *J. Am. Chem. Soc.*, 2005, **127**(23), 8492–8498.

53 G. L. Long and J. D. Winefordner, Limit of Detection A Closer Look at the IUPAC Definition, *Anal. Chem.*, 1983, **55**(07), 712A–724A.

54 J. C. García-Mesa, P. Montoro Leal, M. M. López Guerrero and E. I. Vereda Alonso, Simultaneous determination of noble metals, Sb and Hg by magnetic solid phase extraction on line ICP OES based on a new functionalized magnetic graphene oxide, *Microchem. J.*, 2019, **150**, 104141.

55 J. C. García-Mesa, P. Montoro-Leal, S. Maireles-Rivas, M. M. López Guerrero and E. Vereda Alonso, Sensitive determination of mercury by magnetic dispersive solid-phase extraction combined with flow-injection-cold vapour-graphite furnace atomic absorption spectrometry, *J. Anal. At. Spectrom.*, 2021, **36**(5), 892–899.

56 H. Ahmad, I. I. BinSharfan, R. A. Khan and A. Alsalme, 3D Nanoarchitecture of Polyaniline-MoS_2 Hybrid Material for Hg(II) Adsorption Properties, *Polymers*, 2020, **12**(11), 2731.

57 U. Haseen and H. Ahmad, Preconcentration and Determination of Trace Hg(II) Using a Cellulose Nanofiber Mat Functionalized with MoS_2 Nanosheets, *Ind. Eng. Chem. Res.*, 2020, **59**(7), 3198–3204.

58 A. Cárdenas Valdivia, M. M. López Guerrero, E. I. Vereda Alonso, J. M. Cano Pavón and A. García de Torres, Determination of As, Sb and Hg in water samples by flow injection coupled HR CS ETAAS with an *in situ* hydride generator, *Microchem. J.*, 2018, **138**, 109–115.